Combing and Bending of Carbon Nanotube Arrays with Confined Microfluidic Flow on Patterned Surfaces

Hyunhyub Ko, Sergiy Peleshanko, and Vladimir V. Tsukruk*

Materials Science & Engineering Department, Iowa State University, Ames, Iowa 50011

Received: November 5, 2003

Ordered arrays of carbon nanotubes in bent and straight states were prepared using "wet" deposition of nanotube solutions on a patterned surface. This approach provided a means for the formation of highly oriented and textured nanotube arrays of different types. Moreover, under certain conditions, nanotube loops of different shapes were formed on amine-terminated silicon surface stripes. Atomic force microscopy observations indicated that the majority of the deposited nanotubes (up to 90%) are uniformly oriented and up to 40% of aligned nanotubes are folded into different nanoscale shapes (open and closed loops with 200−300 nm radius of curvature). We suggested that the dewetting of the SAM-confined liquid film was responsible for the alignment of carbon nanotubes and for the formation of the looped nanotubes. The instability of a receding contact line caused water microdroplets behind the dewetting film, which could serve as nuclei for nanotube trapping. The nanotubes pinned to the functionalized surface can be trapped by these drying microdroplets and bent along their shrinking circumference. In addition, highly packed ordered arrays of carbon nanotubes were formed by casting from solution on tilted patterned substrates. The preparation of the ordered arrays of uniform nanotube loops or woven nanotube stripes may be useful in microelectronic and microelectromechanical devices, where tunable electronic and surface properties result from different nanotube shapes, locations, and orientations.

Introduction

As attractive building blocks for molecular electronics, carbon nanotubes (CNTs) have been studied intensely due to their unique structural, mechanical, electrical, and optical properties.[1] Numerous potential applications of CNT-based nanodevices have been proposed including field-effect transistor,[2] field emitter,[3] probe tips,[4,5] chemical sensors,[6,7] and electromechanical sensor.[8] To utilize CNTs in nanodevices, it is necessary to develop efficient strategies for their assembling into hierarchical nanostructures, which could be achieved by controlling the shape, location, and orientation of large nanotube arrays.

Self-organization of CNTs into highly ordered arrays has been approached by direct-growth assembly or post-growth assembly methods. Significant progress in growing vertically aligned nanotube assemblies on patterned substrates has been made recently with pre-catalyst patterning and chemical vapor deposition (CVD).[9−13] Direct-growth assembly by CVD has the advantage of achieving highly ordered and densely packed nanostructures. However, functionalized CNTs can be damaged by the high-temperature CVD process or cannot be synthesized by current CVD methods. Post-growth assembly of CNTs in a vertical direction has been demonstrated by the deposition of CNTs from suspension onto chemically modified surfaces.[14] On the other hand, several in-plane orientation methods have been reported, such as catalytic growth,[15,16] alignment in electric and magnetic fields,[17−19] and self-assembling on chemically modified surfaces.[20−24] Among all these approaches, self-assembly based on wet chemistry has received great attention recently because of the associated mild conditions and the ability to produce well-defined nanostructures.

Recently, the electronic properties of bent and strained carbon nanotubes have been studied with potential applications in mind for electromechanical devices and nanomechanical sensors.[4,25−27] It has been observed that carbon nanotubes, known for their flexibility, can bend elastically,[4,25] and the mechanical deformation strongly affects their electronic properties.[26,27] Therefore, controlled bending and an ordered placement of the bent nanotubes could be interesting for the engineering of electronic properties of nanotube arrays.[28] For instance, as is well-known, the formation of the ring structure of biological macromolecules such as DNA is an efficient way to organize the effective transfer of bioinformation.[29]

In fact, it has been recently observed that microscopic carbon nanotube rings with diameter of about 500 nm are formed by the nanotubes and their bundles during catalytic synthesis or oxidation process.[30−33] The bending mechanism was suggested, which is based on random thermal motion/bending of flexible nanotubes or bubble cavitations. It is believed that the strained shape of the nanotubes immobilized on a solid surface is stabilized by van der Waals interactions or chemical bonding between the tube ends. However, in all cases, only random collections of rings deposited on the solid substrate were observed. Controlled bending has also been achieved with the AFM tip for carbon nanotubes pinned to a silicon surface.[34,35] In this case, the tedious procedure was inherently limited to an individual nanotube and cannot be used to create large-scale arrays of identically bent nanotubes.

In this study, we demonstrate that wet-chemistry approaches (a combination of surface patterning and dip-coating) can be used to produce a massive amount of nanotube loops of different shapes (bent and folded nanotubes, open and closed loops) assembled in horizontally ordered, robust arrays on the patterned

* To whom correspondence should be addressed: E-mail: vladimir@iastate.edu.

10.1021/jp031229e CCC: $27.50
Published on Web 03/13/2004

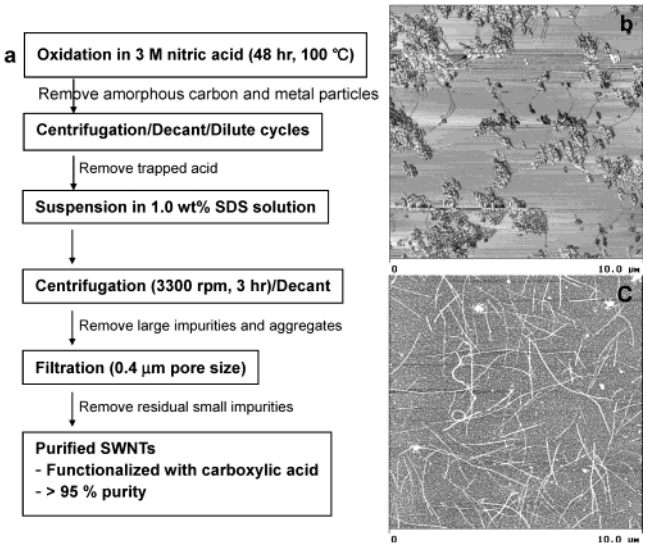

Figure 1. (a) Schematic illustration of the oxidation and purification procedure of carbon nanotubes exploited in this work. Purified CNTs are functionalized with carboxylic acid. AFM topographical images (10×10 μm) of raw CNTs material with impurities (b); purified CNTs with minute fraction of impurities (c). Z-range is 600 nm for (b) and 20 nm for (c).

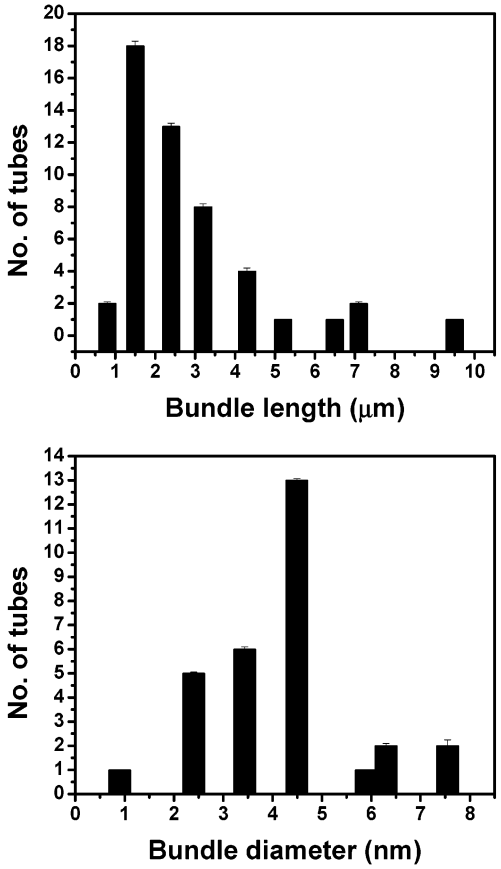

Figure 2. Histograms of size distribution for nanotube bundle lengths and diameters, which shows uniform length (2 ± 0.5 μm) and diameter (3.5 ± 1 nm). Bundle diameters were measured as heights of deposited CNTs from AFM images.

silicon wafer surfaces. This approach provided not only uniform orientation but also well-defined spacing in nanotube positioning on a micron scale controlled by the dimensions of the hydrophilic and hydrophobic patterned surface areas. We propose that the dewetting of the liquid film is responsible for the nanotube alignment and the formation of the looped nanotubes. The bending of the trapped carbon nanotube occurs along the shrinking circumference of the drying liquid microdroplet. We believe that the combination of this newly observed phenomenon with a proper hydrophilic−hydrophobic surface patterning may lead to directed assembly of uniformly looped nanotubes in regular surface arrays.

Experimental Section

Purification. The single walled carbon nanotube (SWNT) raw material, produced by the arc discharge method, was purchased from MER Corporation (Arizona, U.S.A.). The raw material is composed of about 12 wt % SWNTs (1.2−1.4 nm in diameter, 10−50 μm in length, bundles of up to 20 nanotubes), along with other impurities including metal catalyst particles, amorphous carbon, and fullerenes, as can be seen on AFM images of the raw material adsorbed on a silicon surface (Figure 1b). The multistep purification procedure applied here involved oxidation in nitric acid, centrifugation, and filtration,[36,37] as shown schematically in Figure 1a. Sodium dodecyl sulfate (SDS) surfactant (Aldrich) was used to make a stable colloidal suspension of SWNTs.[38] First, 50 mg of raw material was refluxed in 50 mL of 3 M HNO_3 solution for 48 h at 100 °C. After the refluxed material was centrifuged for 30 min at 3300 rpm, the red-brown supernatant acid was decanted off. The trapped acid in the sediment was removed by repeatedly (3−4 times) re-suspending the sediment in Nanopure water (sonication for 2 min), centrifuging, and decanting the supernatant. Next, the sediment was dispersed in 20 mL of 1 wt % aqueous sodium dodecyl sulfate (SDS) surfactant by sonication for 1 h. Immediately after sonication, the resulting dispersion was centrifuged at 3300 rpm for 3 h, and the sediment of undispersed large aggregates was removed. Finally, the suspension was filtered with polycarbonate membranes (0.4 μm pore size, Millipore) for the removal of remaining small impurities. After filtration, the residue on the filter was scraped and dispersed in 10 mL of 1 wt % SDS surfactant by sonication for 1 h. Subsequently, large aggregates of SWNTs in this suspension were removed by centrifugation at 3300 rpm for 1 h. The resulting black supernatant was kept in clean vial for future experiments.

Substrate Patterning. Microcontact printing (μCP) was used for the patterning of self-assembled monolayers (SAMs) on a silicon oxide surface according to the well-established routine.[39−41] A poly(dimethylsiloxane) (PDMS) (Dow Chemical) stamp was cured at 60 °C for 1 h in a vacuum and released from a patterned mold of the highly polished micromachined silicon grid with 10 μm spacing (Micromash). For surface patterning, an octadecyltrichlorosilane (OTS) (Aldrich) toluene solution was used as ink. (Aminopropyl)triethoxysilane (APTS) (Aldrich) SAMs containing amine-terminated groups with the high ability to attract carboxylic groups were used to form hydrophilic stripes on the silicon oxide surface. We routinely used these SAMs for tethering a variety of molecules and nanoscale objects (e.g., polyelectrolytes, dendrimers, and hyperbranched molecules).[42,43] The procedure for μCP and subsequent deposition of carbon nanotubes on the patterned SAMs is shown schematically in Figure 4.

Silicon modification was conducted with a usual procedure adapted in our lab.[42,44] The (100) silicon wafers (Semiconductor Processing) were cut in rectangular pieces of approximately 1×2 cm. They were cleaned in Nanopure water in an ultrasonic bath for 10 min, immersed in a piranha solution (3:1 concentrated sulfuric acid:30% hydrogen peroxide, *health hazard*) for

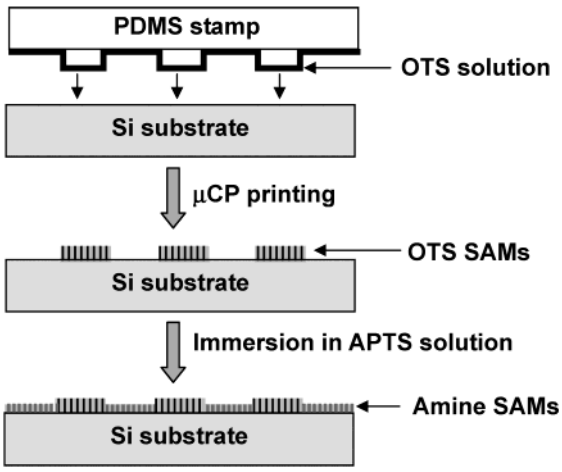

Figure 3. Schematic illustration of surface patterning by microcontact printing technique showing printing of methyl-terminated OTS SAM followed by backfilling with amine-terminated SAM.

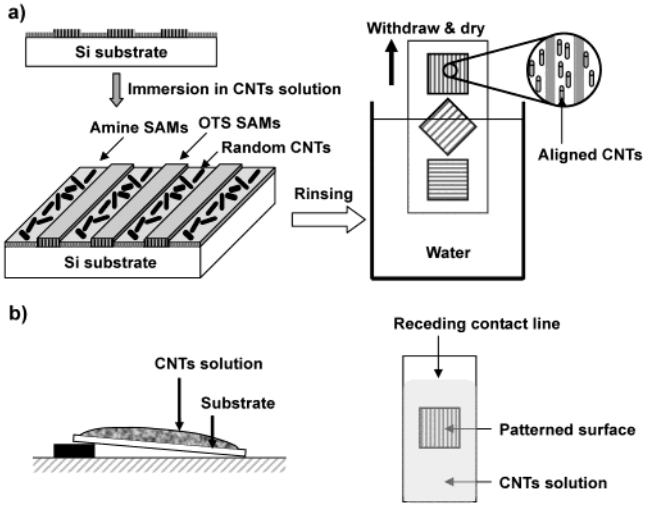

Figure 4. Schematic illustration of the nanotube adsorption from solution on amine-terminated stripes. (a) Dip-coating process: Patterned substrates are immersed horizontally in CNTs solution. CNTs randomly adsorb on amine-terminated stripes during immersion. The substrates are withdrawn vertically from the rinsing reservoir and are dried vertically in ambient laboratory conditions. Three different directions of patterns were tested during a single experimental run. An ordered array of carbon nanotubes is formed during rinsing and drying. (b) Casting of CNTs solution on the patterned substrate. As the solution dewets along the hydrophilic stripes and solvent evaporates, the CNTs are adsorbed along with receding contact line, forming densely packed arrays.

1 h to re-grow the oxide layer, and then rinsed several times with Nanopure water (18 MΩ cm, Nanopure). After rinsing, the substrates were dried under a stream of nitrogen and stored in sealed containers. For the preparation of OTS patterned SAMs, the PDMS stamp was immersed into the 0.5 vol % OTS solution in toluene to ink its surface inside the nitrogen-purged glovebox (<5% RH), moved outside the glovebox in OTS solution, dried with a stream of nitrogen for 30 s, and then brought in contact with the cleaned silicon substrate for 30 s in ambient conditions. After each printing, the PDMS stamp was sonicated in toluene and ethanol for 2 min each and dried with a stream of nitrogen for 1 min to remove contaminations. The patterned samples were rinsed with chloroform and dried with a stream of nitrogen. To amine-terminate, the bare silicon surface areas were backfilled with APTS by immersion in a 1.0 vol % APTS solution in toluene for 10 min after 1 h hydrolysis of APTS solution inside the nitrogen-purged glovebox. Samples were then rinsed with chloroform and dried with nitrogen. All procedures were conducted under cleanroom class 100 conditions to prevent contaminations with external impurities.

Nanotubes Deposition. Figure 4 shows schematically the process of CNTs deposition by dip-coating or casting from solution. For dip-coating (Figure 4a), patterned substrates were immersed horizontally in the carbon nanotubes solution for 24 h, rinsed briefly (~30 s) in Nanopure water, dry-immobilized in ambient laboratory conditions. After this, the substrates were rinsed again in Nanopure water by withdrawing from a rinsing bath and drying vertically. The withdrawing rate was in the range from 1 to 20 mm/s for all cases studied here. Faster withdrawal resulted in irreproducible results, and slower withdrawal resulted in the absence of bent nanotubes. To exclude other factors affecting the alignment, we did not use nitrogen gas when drying the samples. After nanotube deposition, the substrates were stored in a desiccator under dry air conditions before AFM studies. For the casting routine (Figure 4b), several droplets of the CNT solution were spread on a patterned substrate and were allowed to dry at ambient laboratory conditions. The substrate was slightly tilted (~5°) to assist the unidirectional drying conditions. After the solvent was completely evaporated, the substrate was rinsed with Nanopure water and dried in ambient conditions. In the course of studies, we tested the effect of rinsing and mutual orientation of the liquid flow direction and the direction of stripes in surface patterns (Figure 4).

Surface Characterization. Quality of SAM-modified silicon wafers was initially controlled with contact angle measurements. Ellipsometry was used for the control of SAM thickness. Atomic force microscopy (AFM) scanning was performed in the tapping mode on a Dimension 3000 (Digital Instruments, Inc.) microscope under ambient conditions according to the usual experimental procedure adapted in our laboratory.[45,46] Topographical and phase AFM images were acquired at scan rates in the range of 0.5−1.0 Hz and a set-point amplitude ratio of about 0.8−0.9, which corresponded to the light tapping regime. Silicon cantilevers with a spring constant of about 50 N/m and a tip radius of 10−20 nm were used in this study. These parameters were verified by a resonance frequency measurement and a gold nanoparticle reference sample.[47]

Results and Discussion

Purified CNTs. In the raw nanotubes material, individual nanotubes can be found within amorphous material in the form of bundles, which are several hundred micrometers long and are composed of 10−1000 individual nanotubes (Figure 1b). These nanotubes are entangled with impurities in the form of large submicron aggregates. For the proper use of carbon nanotubes in nanodevices, nanotubes should be in the state of separate individual nanotubes and small bundles with proper length and functional groups, which can be used for directed self-assembly of nanotubes. For the preparation of such functionalized nanotubes with high purity, small bundle size, and appropriate length, we used a combined method of multistep purification and oxidation procedures as described above. Oxidation in nitric acid can modify the open ends of nanotubes with carboxylic acid groups, which are capable of strong tethering to the amine surface groups as was demonstrated in several recent publications.[20,42] This interaction is important for tethering of carbon nanotubes to a functionalized surface in addition to conventional side wall−surface interactions. The oxidized nanotubes can be used for further chemical modification or for the attachment to the functionalized surface.

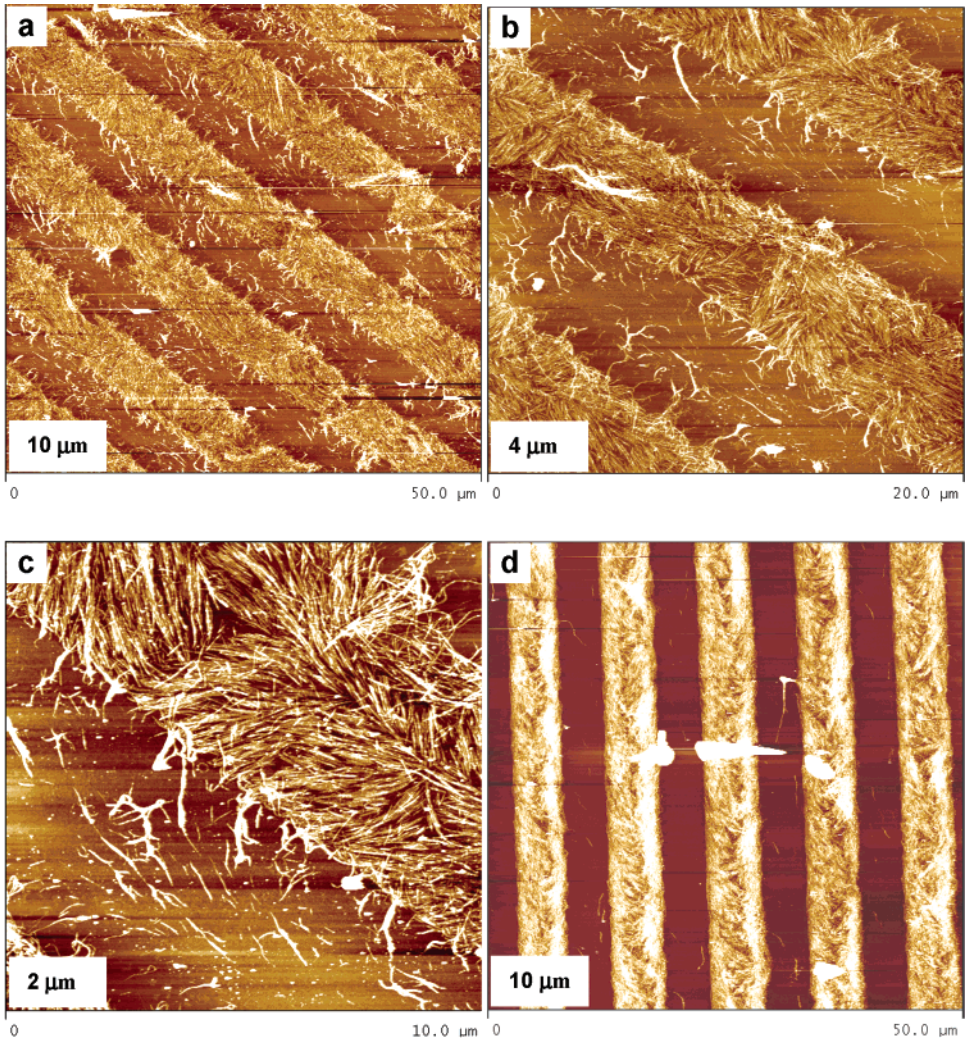

Figure 5. AFM topographical images of adsorbed carbon nanotube arrays on amine-terminated stripes obtained by casting of CNTs solution on patterned substrates. Z-range is 80 nm for 50 × 50 μm images and 40 nm for the other images. Pattern direction is at acute angle (a−c) and parallel (d) to the drying direction.

With this combined procedure, impurities of metal particles, amorphous carbon, and carbon nanoparticles could be effectively removed. In fact, the analysis of purified samples by AFM showed virtually exclusive nanotube material (Figure 1c). The purity of nanotube material used in this study (> 95% of carbon nanotubes and their bundles) was estimated from the apparent surface coverage calculated as the bearing ratio from AFM height histograms using a predefined threshold of 10 nm. Clean carbon nanotube bundles with the average diameter of 3.5 ± 1 nm contained 3−20 nanotubes with the average length of 2 ± 0.5 μm as determined from corresponding length and height histograms (Figure 2).

Nanotube Deposition on Micropatterned Surfaces. For the selective deposition of purified nanotubes, this procedure produced chemically heterogeneous surfaces with well-defined periodicity via the microcontact printing technique in accordance with classical results (Figure 3).[48] The micropatterned surface was composed of alternating hydrophilic and hydrophobic stripes: modestly hydrophilic amine-terminated (−NH_2) SAMs (contact angle of 30−40°) with the ability for strong grafting of carboxyl-functionalized carbon nanotubes and methyl-terminated (−CH_3) SAMs with weak adsorbing ability for various chemical groups and high hydrophobicity (contact angle reaching 120°).[20,42,49] As can be seen in Figure 5, the hydrophilic amine-terminated surface areas are represented by darker stripes of 7 μm width on AFM topographical images. White stripes of about 3 μm across represent thicker hydrophobic methyl-terminated SAM areas (about 1.2 nm thicker as expected for these SAMs and confirmed by AFM [42]).

Figures 5−9 show different types of carbon nanotube arrays on various surfaces (patterned substrates with different directions or nonpatterned amine-modified substrate) under different deposition methods including casting (Figures 5 and 6) or dip-coating (Figures 7−9). Pattern direction, which corresponds to the direction of stripes, varied with respect to the drying direction. We used all acute angle (45°) (Figures 5a−c, 7e), horizontal (Figures 5d, 6, and 7b,d), and vertical (Figure 7a,c) orientations to the drying direction (see sketch in Figure 4). For the dip-coating process, the majority of carbon nanotubes deposited on the patterned substrates with vertical or horizontal orientation to the drying direction and formed dense nanotube assemblies on stripes of amine-terminated SAMs with high selectivity. In fact, very few nanotubes can be found on hydrophobic stripes. The types of orientation and ordering of the carbon nanotubes confined to the "sticky" stripes ranged from preferential orientation of the straight or bent nanotubes stretched along the stripes to "chevron"-like arrays of different densities.

Casting from solution on tilted substrates followed by gentle rinsing resulted in the formation of densely packed arrays of different configurations reminiscent of woven fabrics (Figure 5). The average thickness of these woven stripes stays within

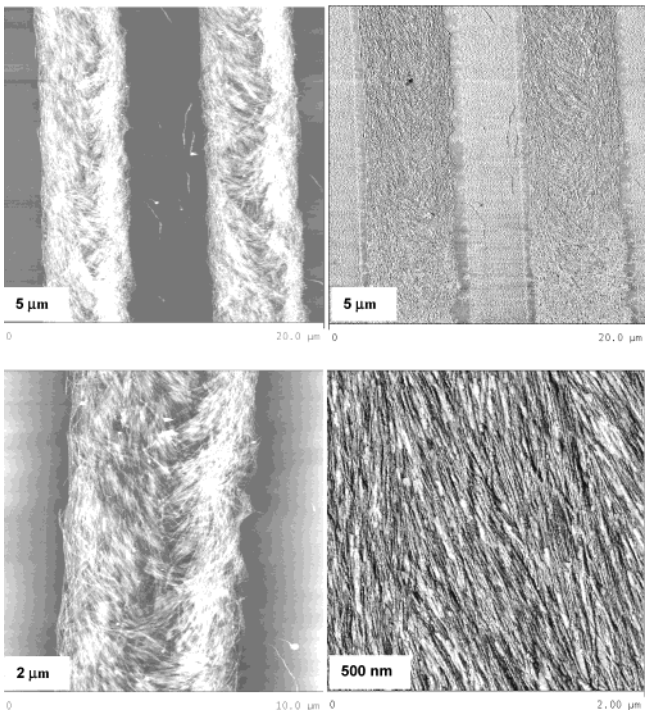

Figure 6. Different scales of AFM topographical (left) and phase (right) images of "woven" texture of carbon nanotube "fabric" on patterned surfaces obtained by casting of CNTs solution. Z-range is 80 nm for topographical images and 20° for phase images. Pattern direction in all cases is parallel to the drying direction.

10−30 nm that indicates multilayered character of the adsorbed material composed of several (3−8) layers of bundles. Under these conditions, very few carbon nanotubes can be found on the hydrophobic surface areas, which demonstrates the high selectivity of the adsorbing process. Woven patterns are very regular, are repeatedly reproduced along the stripes, and are consistently observed for all stripes over millimeter size surface areas under given casting conditions (see several neighboring stripes in Figure 6). The local orientation of carbon nanotube assemblies within these arrays is very uniform with nematic-like ordering of densely packed straight nanotubes expanding over microscopic areas, as can be seen in Figure 6. It is likely that the local nematic ordering with uniform orientational ordering and no positional ordering is caused by higher lateral capillary forces along the length of a nanotube as compared to its width.[50] Before, a similar mechanism of nanotubes nucleation was described in detail by Zhou et al.[21,22]

Combing and Bending of Carbon Nanotubes by Patterned Microfluidic Flow. Dip-coating of patterned substrates resulted in a monolayer coverage of less dense carbon nanotubes on the amine-terminated stripes (Figure 7). An overall ordering pattern of a single layer of nanotubes was similar to the texture of highly packed arrays but without multiple layering of the nanotube bundles. These "monolayer" arrays were firmly tethered to the functionalized silicon surface and cannot be removed with additional rinsing and ultrasonic treatment. This tethering is facilitated by electrostatic attraction, occasional chemical bonding, and strong van der Waals interactions between side walls/tube ends and the substrate.[23,51] The deposition of carbon nanotubes on the patterned substrate oriented by an acute angle to the drying direction resulted in randomly entangled carbon nanotubes stretched along the amine-terminated stripes (Figure 7e). In addition, the deposition of carbon nanotubes on unpatterned amine-terminated surface showed an array of randomly oriented nanotubes without any indication of orientational ordering (Figure 7f). These results demonstrate a critical importance of the surface patterning and its orientation with respect to the drying direction for the formation of regularly oriented arrays of carbon nanotubes.

Detailed analysis of the ordered nanotubes firmly tethered to the amine-terminated surface showed that individual carbon nanotubes within oriented monolayer arrays tend to form a variety of curled shapes (Figure 8). These regularly curled nanotubes are very different from straight rodlike shapes of nanowires observed for arrays fabricated with uni-directional microfluidic flow.[52] Different shapes of nanotube loops (single and double "nooses", completely folded "hooks", nanotube "arches", and sharply folded "needle eyes") are consistently observed on micron scale areas (Figures 8 and 9). On average,

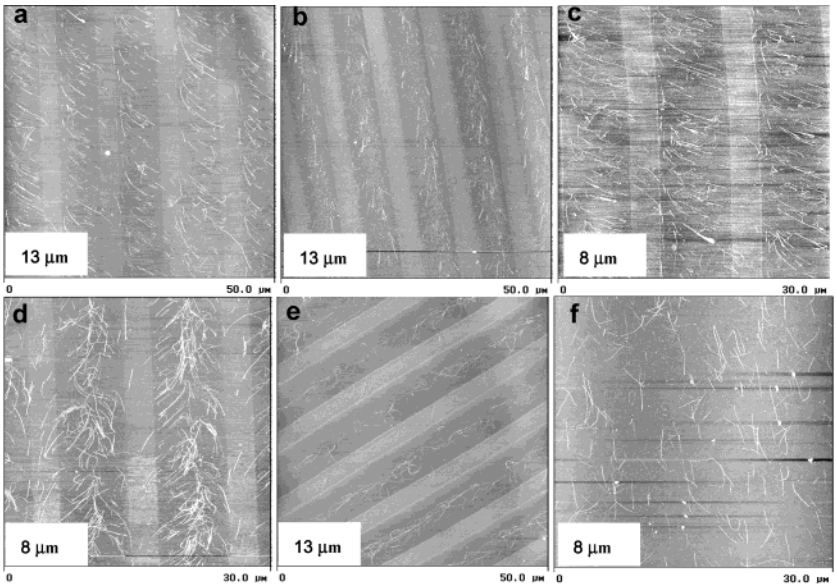

Figure 7. AFM topographical images of ordered arrays of carbon nanotubes on different silicon surfaces obtained by dip-coating: pattern direction is vertical for (a) and (c), parallel for (b) and (d), and at acute angle for (e). Image (f) is a nonpatterned amine-modified surface. Dark and bright stripes represent alternating hydrophilic and hydrophobic surface areas with the microroughness below 0.3 nm within 1×1 μm surface area. The occasional presence of the carbon nanotubes on the hydrophobic stripes is caused by surface imperfections. Z-range is 60 nm for all images.

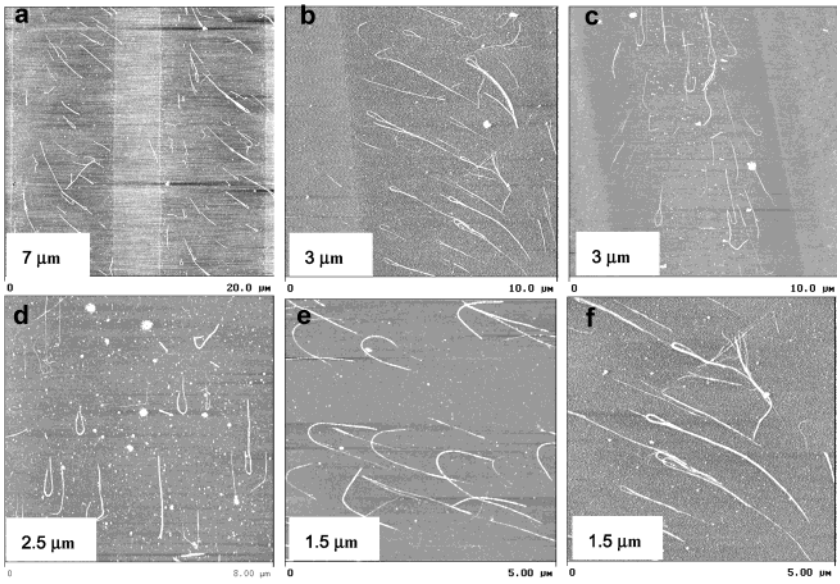

Figure 8. High magnification AFM topographical images of arrays of carbon nanotube loops with different shapes obtained by dip-coating. Z-range is 40 nm for all images. Substrates are vertical (a, b, and f) and perpendicular (c, d, and e) to the drying direction. Withdrawing speed is 10−20 mm/s for a, b, c, d, and f and ∼1 mm/s for e.

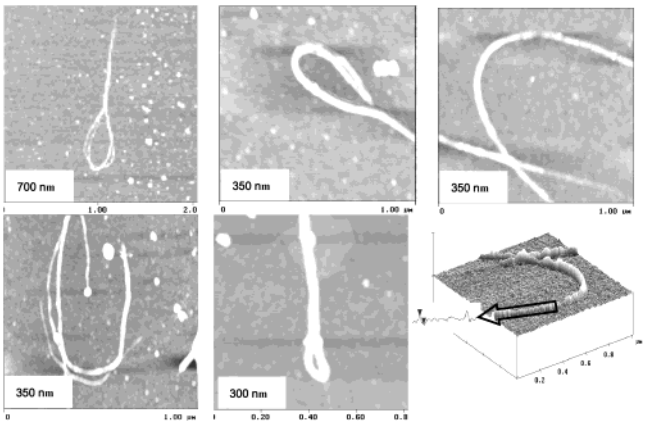

Figure 9. High-resolution AFM topographical images of different types of coiled and folded nanotubes presented in Figure 8 and obtained by dip-coating: top-view images and 3D image with a longitudinal cross section. Z-range is 20 nm for all images.

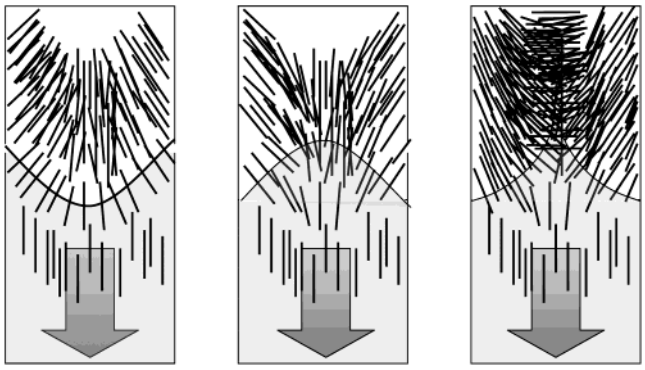

Figure 10. Sketches of the formation of the different textured nanotube arrays by differently shaped meniscus of fluid film dewetting along the amine-terminated stripe during casting process.

between 30 and 40% of all aligned nanotubes for a specific batch are folded in a uniform manner with a high degree of shape persistency over large surface areas with linear density of about one nanotube per micron.

Inspection of the bent nanotubes at high magnification revealed that loops of different types were formed by bending a portion of the nanotube that is typically less than half of its total length (Figure 9). A significant portion of the backward bent tube was in close contact with the straight, un-bent portion. The radius of curvature of the coiled portion was within 200−300 nm and fairly uniform under identical preparation conditions. It is clear that bending and anchoring of the nanotubes under such confined conditions should result in significant local stresses, which could lead to the splitting of the bundles (see "double noose" or split nanotube arches in Figure 9). Nanotube bending frequently causes their sectioning as demonstrated in a selected longitudinal cross section in Figure 9.

Models of Nanotube Surface Behavior. As was shown above, different treatment methods resulted in the formation of different types of nanotube arrays. Thus, we suggested two major and different mechanisms responsible for each result. At first, for the dip-coating process, we propose that the gradient dewetting of the stripped liquid film confined to the hydrophilic stripes is responsible for the alignment of CNTs and the formation of the looped nanotubes in the drying process. When the substrate is withdrawn vertically from a rinsing reservoir, an ultrathin liquid film is formed on the withdrawn substrate.[53] As known, during the drying process of the liquid film on the tilted/vertical substrate under the unidirectional gravitational force, the downwardly dewetting liquid film exerts a hydrodynamic drag force and the receding contact line of this dewetting film exerts a downward surface tension.

We present a sketch of this alignment procedure that includes two different scenarios, combing and bending of nanotubes (Figures 10 and 11). Here, we suggest that the formation of highly textured dense nanotube arrays is facilitated by vertical hydrodynamic forces causing initial orientation of carbon nanotubes along the hydrophilic stripes. Further formation of the orientation texture is controlled by the receding contact line, which aligns all carbon nanotubes perpendicular to the meniscus according to detailed studies on the combing process for rodlike molecules such as DNA.[54] A complex texture is formed by a corresponding complex shape of the meniscus within the confined hydrophilic stripes such as presented in Figure 10 for some examples. The meniscus shapes presented here are, in fact, responsible for several specific textures observed experimentally. This mechanism is virtually identical to that suggested for DNA

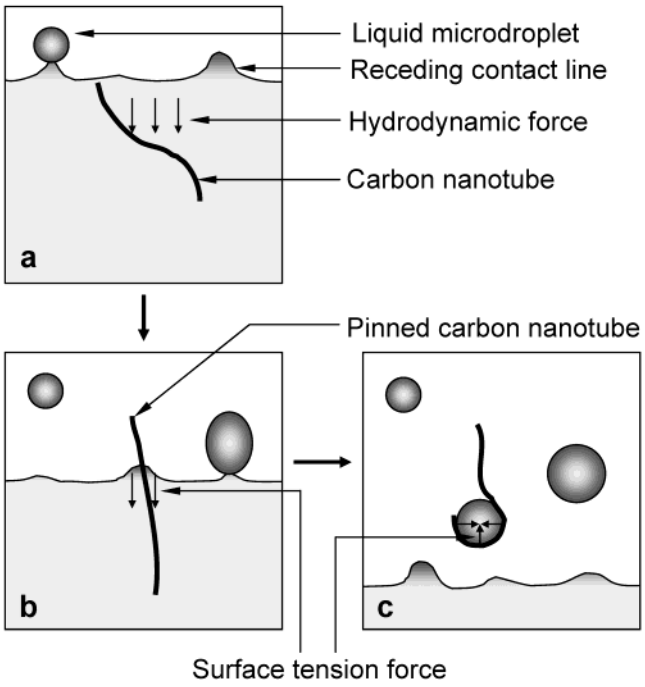

Figure 11. Schematic of alignment and bending mechanism by the instabilities of the receding contact line: (a) contact line instability and randomly oriented carbon nanotube; (b) ordering of carbon nanotube by the receding contact line front; (c) trapping and initial bending of carbon nanotube by the liquid microdroplet left behind the receding contact line.

combing with the only significant difference being a manner of the creation of microfluidic patterned flow not within closed microchannels but directly on an open patterned surface of silicon wafers.

The process of nanotube bending during treatments includes a more complex series of surface phenomena as suggested in Figure 11. During initial immersion of the substrate in solution, CNTs are randomly attached to the amine-terminated surface mainly by their functionalized ends. Also, nanotube sidewalls can be tethered to the amine-terminated surface via electrostatic interactions facilitated by surfactant SDS linkers. It can be expected that tethered nanotubes are mobile in the solution as the surfactant molecules are removed in the course of careful rinsing routine. When the substrate is affected by the unidirectional water flow during the rinsing stage, the meniscus moves upward with the substrate forming a thin liquid film. This liquid film dewets instantaneously on OTS-covered stripes because of their hydrophobicity, thus forming a stripped flow pattern concentrated along the hydrophilic stripes. As the liquid film is drying, the dewetting liquid film exerts a hydrodynamic drag force on the anchored nanotubes. Also, the receding contact line exerts a downward local force on the immersed part of each anchored nanotube, while the emerged nanotubes remain immobilized to the substrates. The instability of the receding contact line (solid-fluid-air) causes periodically spaced water microdroplets left behind the receding contact line.[55,56] Unlike the previous scenario, the pinned nanotube can be trapped by these drying microdroplets caused by contact line instabilities and initially align themselves along the droplet circumference in a straight form (Figure 11).

At the next stage of microdroplet drying, the decreasing of the overall circumference along with increasing of its curvature force the trapped carbon nanotubes to follow the overall diminishing shape of the droplets by gradual bending (Figure 12). Eventually, at later stages of drying, the nanotube bends

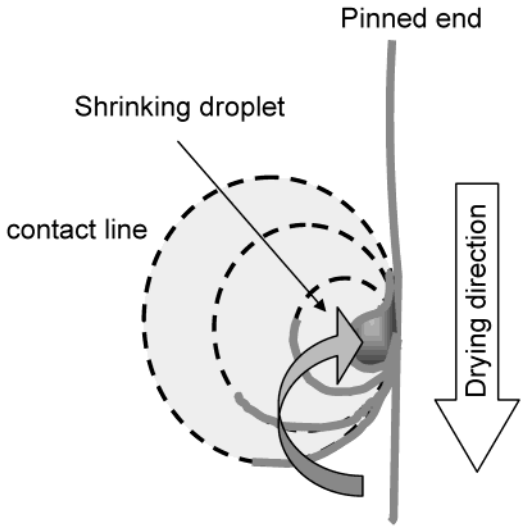

Figure 12. Schematic of the suggested mechanism of pinned and trapped nanotube bending with a moving receding front of the drying microdroplet. The loop orientation depends on initial angle between the trapped nanotube and the direction of the gravitational force and can vary in a wide range.

back on itself. The free end of the nanotube completes a full 180° bending and meets the un-bent portion of the nanotube stabilized by the pinned end. At this point, further folding stops because of increasing bending resistance due to a physical obstacle (Figure 12). The nanotube loops are fixed in this strained state by strong interactions with the functionalized substrate and van der Waals interaction between the two portions of the nanotube in a close contact. The variation of the initial trapping scenarios and size/location of the microdroplet array causes a variety of looped shapes formed under different preparation conditions.

Let's consider how these findings correspond to the known data. Previously, the ability of a receding contact line to align carbon nanotubes was demonstrated on the PDMS micromold surfaces,[57] homogeneously modified silicon surfaces,[24] or more recently on the patterned glass surfaces.[22] These studies were mainly focused on the alignment of straight carbon nanotubes and the proposed mechanism could well explain the alignment of straight carbon nanotubes similarly to that presented in Figure 10. Bensimon et al. reported alignment, stretching, and bending of DNA molecules with a receding meniscus and proposed the pinned DNA molecules become attached to a solid surface.[58−60] On the other hand, the mechanism of the surface trapping of carbon nanotubes by the micro-bubbles in ultrasonically treated solution and their bending during cavitation and bubble collapse was suggested as an explanation for the ring formation.[30,31] Also, ring-shaped structures of nanoparticles (nanocrystals, porphyrin molecules, carbon nanotubes) were explained by the nucleation and growth of holes in an evaporating liquid film.[61] All of these experiments show that the surface tension force could cause ordering of nanotube arrays under proper conditions.

Indeed, we noted before that the periodically patterned substrate is crucial for the formation of the ordered arrays of nanotube loops. Nanotube assembly on the nonpatterned amine-terminated surface resulted in random surface arrays. As mentioned above, the instabilities of the receding contact line caused the formation of an unstable contact line. On a patterned surface, the receding contact line shape is uneven along the whole patterned area due to the confinement by alternating hydrophilic and hydrophobic stripes, causing an array of small liquid microdroplets left behind. Thus, on the patterned surface,

nanotubes aligning perpendicular to the meniscus direction are organized into uniform ordered arrays. As the stripe width increases, the contact line shape becomes more uniform.[53] Therefore, on the nonpatterned amine-terminated surface with no confinement on liquid flow, the receding contact line shape of drying liquid film will be more uniform with lower chances for microscale instabilities.

In suggested mechanisms of nanotube orientation, two main forces acting on anchored nanotubes are the surface tension and the hydrodynamic force. As known, the surface tension on the patterned surface can be evaluated as $F_s \approx \gamma\ \pi$D where γ is the surface tension of the liquid and D is a nanotube diameter.[62] Estimation for $D = 3.5$ nm for the nanotube bundle gives $F_s \approx 0.8$ nN. On the other hand, the hydrodynamic drag force is defined as $F_h \approx \eta l$V, where η is the liquid viscosity, l is the nanotube length, and V is the velocity.[63] Ignoring the contribution of the gravitational force, the velocity of the hydrodynamic flow can be estimated as the rate of dewetting, $V = \gamma\theta^3/6\eta L$ where θ is the contact angle of the liquid formed on the substrate and L is a constant of order 10.[55,64] Note that the velocity of the hydrodynamic flow is not a substrate withdrawing speed, but the rate of dewetting during the drying process. Taking $\eta = 0.01$ P for water, $l = 2\ \mu$m, $\gamma = 72.75 \times 10^{-3}$ N/m, and $\theta = 60°$ (measured for the overall patterned areas), F_h can be estimated to be close to 3 nN, which is higher than the surface tension force estimated above (0.8 nN). Thus, nanotubes can be aligned along the direction of the hydrodynamic force. The hydrodynamic force on the amine-modified substrate ($\theta = 30-40°$) is estimated to be about 1 nN, which is also strong enough to align the carbon nanotubes. However, the final formation of the nanotubes array (ordered or random) follows the path dictated by the surface tension. It can be explained that, even though nanotubes are aligned by strong hydrodynamic force, the surface tension at the contact line reorients the nanotubes before their immobilization on the surface.

We suggested that different shapes of bent nanotubes were due to the variation of the initial trapping scenario and both size and location of the microdroplets left behind the receding contact line. In addition, our experimental result (Figure 7f) shows that the nanotube loops are not formed on the nonpatterned amine-terminated surface. We suggest that this due to the fact that the microdroplets of a proper size are not formed during dewetting under these conditions. In fact, the mean size of the liquid microdroplets is proportional to the liquid film thickness,[55] which is affected by withdrawing speed, inclination angle, and the surface wettability.[53] Hence, with the other conditions the same, the average size of the microdroplets on the nonpatterned amine-terminated substrate will be much larger than that of the patterned substrate. Keeping in mind that possible bending of carbon nanotubes can arise when the size of the shrinking microdroplets is below some critical size comparable with the length of the nanotubes, we conclude that dewetting conditions on the nonpatterned amine-modified substrate are not favorable for nanotube trapping.

The mechanism of nanotube looping suggested here could be valid only if the surface tension acting along the shrinking contact line of the microdroplet outweighs strain forces arising from nanotube bending. The evaluation of the surface tension, which arises from the shrinking contact line,[62] leads to the conclusion that only elastic rods with a spring constant higher than 1−5 N/m could sustain the pressure across the curved contact line. On the other hand, the evaluation of the bending properties required for nanotube folding can be conducted using the known value of the elastic modulus, $E \sim 1$ TPa.[25,65,66] A spring constant, K, for the nanotube portion participating in the continuous bending can be determined within the solid rod approximation by using the equation $K = 3\pi R^4 E/4L^3$, where R is the bundle radius and L is the length of the curved potion.[67] Estimation for $L = 0.3-1\ \mu$m and $R = 1-2$ nm gives values close to 10^{-2} N/m, which is well below the critical stiffness of 1−5 N/m required to prevent tube bending. Thus, the pinned carbon nanotube aligned along the fluid-air-solid interface can be easily bent by the shrinking contact line of the microdroplet.

Conclusions

In this work, we presented a detail discussion of a controlled patterning and shaping of carbon nanotube arrays recently discovered in our group.[68] We demonstrated that a wet-chemistry approach can be used to produce a massive amount of textured nanotube fabrics or nanotube loops of different shapes (bent and folded nanotubes, open and closed loops) assembled in ordered, robust arrays on the patterned silicon wafer surface. We suggest that the phenomenon observed here is related to the rodlike molecule orientation by the contact liquid−air line observed in combing of DNA molecules. The contact line instabilities generate an array of microdroplets behind the receding liquid front. Nanotubes can be trapped by these microdroplets and bent along their shrinking circumference during the drying process. This phenomenon is responsible for the formation of a massive amount of regularly bent nanotubes concentrated along the hydrophilic stripes on the patterned silicon surface extended over millimeter size areas. We would like to emphasize that the orientation and bending mechanisms are facilitated by the pinning of the carbon nanotubes predominantly tethered to the functionalized surface by their carboxylic end groups. Different nanoscale shapes of the nanotube loops are caused by a variable size of the microdroplets left behind the receding contact line. In the end, the nanotube loops are fixed in the strained state by strong van der Waals interactions of nanotube walls and surfactant molecules with the functionalized substrate enhanced by tethering of the nanotube ends.

Finally, it is worth noting how the mechanism responsible for the nanotube array formation by solution casting on the tilted substrate is different from that facilitated by dip-coating. For the dip-coating process, nanotubes are initially adsorbed during immersion and then aligned during the drying process by combined hydrodynamic and capillary forces. However, for the casting process, nanotubes adsorption and alignment arise at the same time, resulting in highly packed nanotube arrays. In casting on the tilted surface, the liquid film spontaneously sweeps down at the patterned substrate, rising the solution concentration along the hydrophilic stripes. Successive drying of this liquid film causes nanotubes deposition by the nucleation along the contact line. In this case, the nanotubes align parallel to the contact line. In our experiments, spontaneous dewetting of CNTs solution and heterogeneity on the patterned surface cause a complex and variable contact line shape and, thus, various types of highly packed nanotube arrays. We can speculate that these arrays can be created even in a more regular manner by using auto-condensation and organized de-wetting phenomena leading to the formation of ordered arrays of microdroplets with a well-defined spacing.[69,70]

Acknowledgment. This work is supported by the NASA through NDE Center Contract NAG 102098, NSF with CMS-0099868 and CTS-0210005 Grants, and AFOSR, F496200210205 Grant.

References and Notes

(1) Baughman, R. H.; Zakhidov, A. A.; de Heer, W. A. *Science* **2002**, *297*, 787.

(2) Tans, S. J.; Verschueren, A. R. M.; Dekker, C. *Nature* **1998**, *393*, 49.

(3) Rinzler, A.; Hafner, J. H.; Nikolaev, P.; Lou, L.; Kim, S. G.; Tomanek, D.; Nordlander, P.; Colbert, D. T.; Smalley, R. E. *Science* **1995**, *269*, 1550.

(4) Dai, H.; Hafner, J. H.; Rinzler, A. G.; Colbert, D. T.; Smalley, R. E. *Nature* **1996**, *384*, 147.

(5) Wong, S. S.; Joselevich, E.; Woolley, A. T.; Cheung, C. L.; Lieber, C. M. *Nature* **1998**, *394*, 52.

(6) Kong, J.; Franklin, M. R.; Zhou, C.; Chapline, M. G.; Peng, S.; Cho, K.; Dai, H. *Science* **2000**, *287*, 622.

(7) Collins, P. G.; Bradley, K.; Ishigami, M.; Zettl, A. *Science* **2000**, *287*, 1801.

(8) Tombler, T. W.; Zhou, C.; Alexseyev, L.; Kong, J.; Dai, H.; Liu, L.; Jayanthi, C. S.; Tang, M.; Wu, S. Y. *Nature* **2000**, *405*, 769.

(9) Vajtai, R.; Wei, B. Q.; Zhang, Z. J.; Jung, Y.; Ramanath, G.; Ajayan, P. M. *Smart Mater. Struct.* **2002**, *11*, 691.

(10) Zhang, X.; Cao, A.; Li, Y.; Xu, C.; Liang, J.; Wu D.; Wei, B. *Chem. Phys. Lett.* **2002**, *351*, 183.

(11) Cao, A.; Wei, B.; Jung, Y.; Vajtai, R.; Ajayan, P. M.; Ramanath, G. *App. Phys. Lett.* **2002**, *81*, 1297.

(12) Huang, S.; Mau, A. W. H.; Turney, T. W.; White, P. A.; Dai, L. *J. Phys. Chem. B* **2000**, *104*, 2193.

(13) Li, J.; Papadopoulos, C.; Xu, J. M.; Moskovits, M. *Appl. Phys. Lett.* **1999**, *75*, 367.

(14) Cai, L.; Bahr, J. L.; Yao, Y.; Tour, J. M. *Chem. Mater.* **2002**, *14*, 4235.

(15) Kong, J.; Zhou, C.; Morpurgo, A.; Soh, H. T.; Quate, C. F.; Marcus, C.; Dai, H. *Appl. Phys. A: Mater. Sci. Process* **1999**, *69*, 305.

(16) Huang, S.; Cai, X.; Liu, J. *J. Am. Chem. Soc.* **2003**, *125*, 5636.

(17) Krupke, R.; Hennrich, F.; Weber, H. B.; Beckmann, D.; Hampe, O.; Malik, S.; Kappes, M. M.; Lohneysen, H. V. *Appl. Phys. A* **2003**, *76*, 397.

(18) Ural, A.; Li, Y.; Dai H. *Appl. Phys. Lett.* **2002**, *81*, 3464.

(19) Fischer, J. E.; Zhou, W.; Vavro, J.; Llaguno, M. C.; Guthy, C.; Haggenmueller, R.; Casavant, M. J.; Walters, D. E.; Smalley, R. E. *J. Appl. Phys.* **2003**, *93*, 2157.

(20) Liu J.; Casavant, M. J.; Cox, M.; Walters, D. A.; Boul, P.; Lu, W.; Rimberg, A. J.; Smith, K. A.; Colbert D. T.; Smalley, R. E. *Chem. Phys. Lett.* **1999**, *303*, 125.

(21) Shimoda, H.; Oh, S. J.; Geng, H. Z.; Walker, R. J.; Zhang, X. B.; McNeil, L. E.; Zhou, O. *Adv. Mater.* **2002**, *14*, 899.

(22) Oh, S. J.; Cheng, Y.; Zhang, J.; Shimoda, H.; Zhou, O. *Appl. Phys. Lett.* **2003**, *82*, 2521.

(23) Burghard, M.; Duesberg, G.; Philipp, G.; Muster, J.; Roth, S. *Adv. Mater.* **1998**, *10*, 584.

(24) Gerdes, S.; Ondarcuhu, T.; Cholet, S.; Joachim, C. *Europhys. Lett.* **1999**, *48*, 292.

(25) Wong, E. W.; Sheehan, P. E.; Lieber, C. M. *Science* **1997**, *277*, 1971.

(26) Minot, E. D.; Yaish, Y.; Sazonova, V.; Park, J.-Y.; Brink, M.; McEuen, P. L. *Phys. Rev. Lett.* **2003**, *90*, 156401.

(27) Maiti, A. *Nat. Mater.* **2003**, *2*, 440.

(28) Rotkin S.; Gogotsi, Yu. *Mater. Res. Inn.* **2002**, *5*, 191.

(29) Whitesides, G. M.; Mathias, J. P.; Seto, C. T. *Science* **1991**, *254*, 1312.

(30) Martel, R.; Shea, H. R.; Avouris, P. *Nature* **1999**, *398*, 299.

(31) Martel, R.; Shea, H. R.; Avouris, P. *Phys. Chem. B* **1999**, *103*, 7551

(32) Sano, M.; Kamino, A.; Okamura, J.; Shinkai, S. *Science* **2001**, *293*, 1299.

(33) Ahlskog, M.; Seynaeve, E.; Vullers, R. J. M.; Van Haesendonck, C.; Fonseca, A.; Hernadi, K.; Nagy, J. B. *Chem. Phys. Lett.* **1999**, *300*, 202.

(34) Falvo, M. R.; Clary, G. J.; Taylor, R. M., II; Chi, V.; Brooks, F. P., Jr.; Washburn, S.; Superfine, R. *Nature* **1997**, *389*, 582.

(35) Hertel, T.; Martel, R.; Avouris, P. *J. Phys. Chem. B* **1998**, *102*, 910.

(36) Liu, J.; Rinzler, A. G.; Dai, H.; Hafner, J. H.; Bradley, R. K.; Boul, P. J.; Lu, A.; Iverson, T.; Shelimov, K.; Huffman, C. B.; Rodriguez-Macias, F.; Shon, Y.-S.; Lee, T. R.; Colbert, D. T.; Smalley, R. E. *Science* **1998**, *280*, 1253.

(37) Dujardim, E.; Ebbesen, T. W.; Krishnan, A.; Treacy, M. M. J. *Adv. Mater.* **1998**, *10*, 611.

(38) Bonard, J.-M.; Stora, T.; Salvetat, J.-P.; Maier, F.; Stöckli, T.; Duschl, C.; Forro, L.; de Heer, W. A.; Chatelain, A. *Adv. Mater.* **1997**, *9*, 827.

(39) Xia, Y.; Mrksich, M.; Kim, E.; Whitesides, G. M. *J. Am. Chem. Soc.* **1995**, *117*, 9576.

(40) Jeon, N. L.; Finnie, K.; Branshaw, K.; Nuzzo, R. G. *Langmuir* **1997**, *13*, 3382.

(41) Geissler, M.; Bernard, A.; Bietsch, A.; Schmid, H.; Michel, B.; Delamarche, E. *J. Am. Chem. Soc.* **2000**, *122*, 6303.

(42) (a) Tsukruk, V. V.; Bliznyuk, V. N. *Langmuir* **1998**, *14*, 446. (b) Bliznyuk, V. N.; Everson, M. P.; Tsukruk, V. V. *J. Tribol.* **1998**, *120*, 489.

(43) (a) Tsukruk, V. V. *Prog. Polym. Sci.* **1997**, *22*, 247. (b) Tsukruk, V. V.; Rinderspacher, F.; Bliznyuk, V. N. *Langmuir* **1997**, *13*, 2171. (c) Tsukruk, V. V.; Bliznyuk, V. N.; Visser, D. W.; Campbell, A. L.; Bunning, T.; Adams, W. W. *Macromolecules* **1997**, *30*, 6615. (d) Tsukruk, V. V.; Shulha, H.; Zhai, X. *Appl. Phys. Lett.* **2003**, *82*, 907. (e) Zhai, X.; Peleshanko, S.; Klimenko, N. S.; Genson, K. L.; Vortman, M. Ya.; Shevchenko, V. V.; Vaknin, D.; Tsukruk, V. V. *Macromolecules* **2003**, *36*, 3101.

(44) Luzinov, I.; Julthongpiput, D.; Liebmann-Vinson, A.; Cregger, T.; Foster, M. D.; Tsukruk, V. V. *Langmuir* **2000**, *16*, 504.

(45) Tsukruk, V. V. *Rubber Chem. Technol.* **1997**, *70*, 430.

(46) Tsukruk, V. V.; Reneker, D. H. *Polymer* **1995**, *36*, 1791.

(47) Hazel, J. L.; Tsukruk, V. V. *Thin Solid Films* **1999**, *339*, 249.

(48) Xia, Y.; Mrksich, M.; Kim, E.; Whitesides, G. M. *J. Am. Chem. Soc.* **1995**, *117*, 9576.

(49) Tsukruk, V. V. *Adv. Materials*, **2001**, *13*, 95.

(50) Nikoobakht, B.; Wang, Z. L.; El-Sayed, M. A. *J. Phys. Chem. B* **2000**, *104*, 8635.

(51) Tsukruk, V. V.; Everson, M. P.; Lander, L. M.; Brittain, W. J. *Langmuir* **1996**, *12*, 3905.

(52) Huang, Y.; Duan, X.; Wei, Q.; Lieber, C. M. *Science* **2001**, *291*, 630.

(53) Darhuber, A. A.; Troian, S. M.; Davis, J. M.; Miller, S. M.; Wagner, S. *J. Appl. Phys.* **2000**, *88*, 5119.

(54) Petit, C. A. P.; Carbeck, J. D. *Nano Lett.* **2003**, *3*, 1141.

(55) Reiter, G.; Sharma, A. *Phys. Rev. Lett.* **2001**, *87*, 166103.

(56) Diez, J. A.; Kondic, L. *Phys. Rev. Lett.* **2001**, *86*, 632.

(57) Chen, J.; Weimer, W. A. *J. Am. Chem. Soc.* **2002**, *124*, 758.

(58) Bensimon, A.; Simon, A.; Chiffaudel, A.; Croquette, V.; Heslot, F.; Bensimon, D. *Science* **1994**, *265*, 2096.

(59) Bensimon, D.; Simon, A. Croquette, J., V.; Bensimon, A. *Phys. Rev. Lett.* **1995**, *74*, 4754.

(60) Michalet, X.; Ekong, R.; Fougerousse, F.; Rousseaux, S.; Schurra, C.; Hornigold, N.; Slegtenhorst, M. V.; Wolfe, J.; Povey, S.; Beckmann, J. S.; Bensimon, A. *Science* **1997**, *277*, 1518.

(61) Vossmeyer, T.; Chung, S.-W.; Gelbart, W. M.; Heath, J. R. *Adv. Mater.* **1998**, *10*, 351.

(62) Adamson, A. W. *Physical Chemistry of Surfaces*; John Wiley & Sons: New York, 1990.

(63) White, F. M. *Fluid Mechanics*; McGraw-Hill: New York, 1979.

(64) Redon, C.; Brochard-Wyart, F.; Rondelez, F. *Phys. Rev. Lett.* **1991**, *66*, 715.

(65) Salvetat, J.-P.; Bonard, J.-M.; Thomson, N. H.; Kulik, A. J.; Forró, L.; Benoit, W.; Zuppiroli, L. *Appl. Phys. A* **1999**, *69*, 255.

(66) Walters, D. A.; Ericson, L. M.; Casavant, M. J.; Liu, J.; Colbert, T.; Smith, K. A.; Smalley, R. E. *Appl. Phys. Lett.* **1999**, *74*, 3803.

(67) Beer, F. P.; Johnston, E. R. *Mechanics of Materials*; McGraw-Hill: New York, 1992.

(68) Tsukruk, V. V.; Ko, H.; Peleshanko, S. *Phys. Rev. Lett.* **2004**, *92*, 065502.

(69) Karthaus, O.; Maruyama, N.; Cieren, X.; Shimomura, M.; Hasegawa, H.; Hashimoto, T. *Langmuir* **2000**, *16*, 6071.

(70) Karthaus, O.; Gracjo, L.; Maruyama N.; Shimomura, M. *Chaos* **1999**, *9*, 308.